Title

Evaluation of complex conjugate artifact removal methods used in spectrometer-based Fourier-domain optical coherence tomography systems: a comparative study

ISBN

9780819479501

Authors

Kim, Dae Yu
Werner, John S
Zawadzki, Robert J

Publication Date

2010-02-11

DOI

10.1117/12.842930

Peer reviewed

Evaluation of Complex Conjugate Artifact Removal Methods Used in Spectrometer-based Fourier-domain Optical Coherence Tomography Systems – A Comparative Study

Dae Yu Kim *[a, b], John S. Werner [a, b], Robert J. Zawadzki [a]
[a]Vision Science and Advanced Retinal Imaging Laboratory, Dept. of Ophthalmology, UC Davis Medical Center, 4860 Y Street, Suite 2400, Sacramento, CA 95817;
[b]Dept. of Biomedical Engineering, University of California Davis, Davis, CA 95616

ABSTRACT

We evaluated several, previously published, complex conjugate artifact removal methods and algorithms that have been proposed for Fourier domain optical coherence tomography (Fd-OCT). To ensure comparable conditions, only one OCT system was used, but with modified data acquisition schemes, depending on the requirements of each method/algorithm. This limited our evaluation to single spectrometer based Fd-OCT approaches. The suppression ratio of complex conjugate artifact images using a paperboard is assessed for all tested methods. Several other metrics are also used for comparison, including a list of additional hardware requirements (beyond standard Fd-OCT components) and data acquisition schemes. Finally, *in vivo* human finger pad and nail images are presented for comparison to the standard Fd-OCT images and full-range images.

Keywords: optical coherence tomography, imaging system, medical optics instrumentation, complex conjugate

1 INTRODUCTION

Fourier-domain OCT (Fd-OCT) [1-3], has become the technique of choice over time-domain OCT first introduced in 1991 [4] due to improved acquisition speed and sensitivity. However, a major limitation of this technique is that the Fourier transform of the real spectral signal from the sensor results in two symmetric “mirror” images of the sample structure, the so-called complex conjugate image. This limits the usable imaging depth of the instrument. In order to overcome this drawback, a variety of methods have been suggested to achieve full-range Fourier-domain OCT (mirror artifact-free images). The common theme of many of these techniques focuses on reconstructing complex representations of the "real" spectral fringes acquired by the OCT detector. Historically, the first phase-shifting method was demonstrated to acquire the full-range image of the porcine eye's anterior chamber *in vitro* [5]. Since then, several phase-shifting techniques with a piezoelectric actuator (PZT) [6-8], an electro-optic phase modulator [9,10] and an acousto-optic modulator [11] were developed for eliminating the mirror image. Recently, another method used phase-shifting introduced by pivot offset scanning the sample [12,13] and reference arm mirror [14]. In addition to "active" phase-shifting techniques, several "passive" methods that include implementation of 3x3 fiber optics coupler were presented [15,16]. However due to multiple detector requirements they are naturally better suited for swept-source rather than spectrometer-based Fd-OCT. Additionally, a technique using non-matched dispersion between sample and reference arm has been proposed [17].

In this paper we focus on evaluation of single spectrometer based Fd-OCT approaches only. This is because of our lab experience in this type of instrumentation and we think that these methods have the greatest potential for broad implementation. Three methods are used for phase-shifting techniques which include pivot offset scanning of the sample arm and the reference arm, as well as phase-shifting with the piezoelectric actuator (PZT). The suppression ratio of complex conjugate artifact free images using a paperboard is assessed for all tested methods. Standard Fd-OCT images and full-range images are shown as different acquisition speeds. In addition, the image quality and hardware requirements (beyond standard Fd-OCT components) are compared for the different phase-shifting procedures.

* dyukim@ucdavis.edu; phone 1 916 734-5839; fax 1 916 734-4543; http://vsri.ucdavis.edu/

Optical Coherence Tomography and Coherence Domain Optical Methods in Biomedicine XIV, edited by Joseph A. Izatt, James G. Fujimoto, Valery V. Tuchin, Proc. of SPIE Vol. 7554, 75542X · © 2010 SPIE
CCC code: 1605-7422/10/$18 · doi: 10.1117/12.842930

2 MATERIALS AND METHODS

We implemented three different phase-shifting techniques using pivot offset galvo scanning at the sample arm, pivot offset galvo scanning at the reference arm, and the piezoelectric translator/actuator (PZT). In order to remove the complex conjugate artifacts, we used complex representation of the OCT intensity spectrum which includes linear phase shifts between consecutive A-scans. Full-range images can be achieved by using Fourier filtering processing [18].

2.1 Experimental system

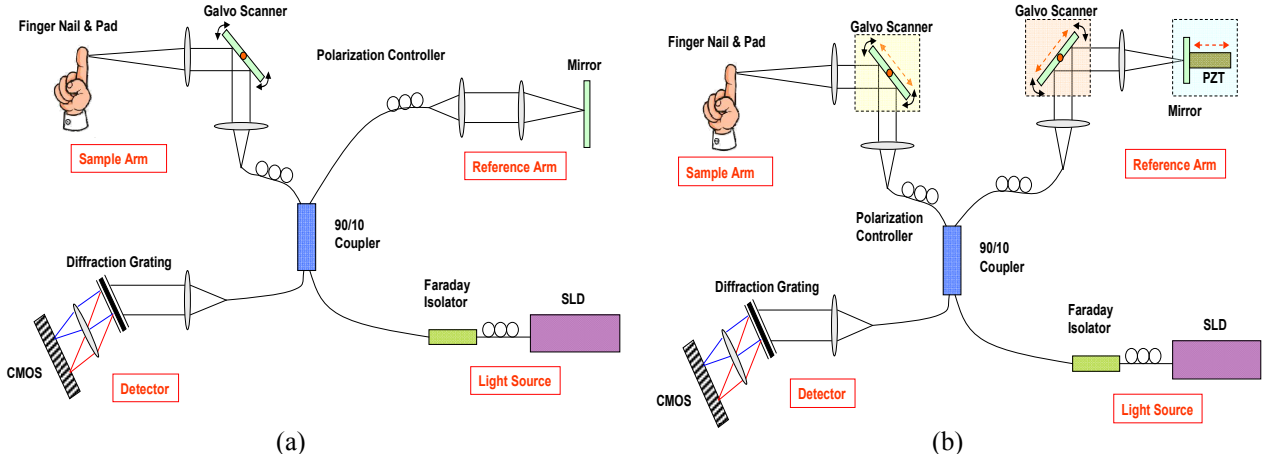

Figure 1. Schematic of the standard Fd-OCT instrument (a) and implemented Fd-OCT used for complex conjugate removal methods and algorithm testing (b). Three dotted rectangles (yellow, pink, blue) in (b) show components that were used to introduce phase shifts: SLD (Superluminescent diode), CMOS (Complementary Metal Oxide Semiconductor), line detecter; PZT, Piezoelectric actuator.

A superluminescent diode with an 890 nm central wavelength (140 nm FWHM) was used as a light source. A Michelson interferometer was used with a sample and a reference (reflecting mirror) arm. A 90/10 fiber coupler sent ten percent of the light toward the sample arm and the beam output power of the sample arm was 450 μW. Light reflected from the sample was combined with the light from the reference mirror, and then sent to a spectrometer where the CMOS line detector (spL4096-140km, Basler), maximum 140 kHz line rate at 4096 pixels and 10x10 μm line pixels, acquired spectral fringes of the light. Operating conditions of the detector were 4 Tap 12 Bit, 80 MHz Camera link clock, and line averaging mode (dual line: 10x20 μm). B-scan imaging frame rates (frames/s) were 100-, 50- and 20 fps for 1000 A-scans using 2048 detector pixels. The optical components of the spectrometer consisted of a 75 mm focal length collimator, a 1200 line/mm volume holographic diffraction grating, and an f=100 mm achromatic objective lens. As shown in Figure 1. (b), the testbed of the sample arm scanner as well as the reference arm scanner can be used to introduce phase shifts for the complex conjugate removal algorithm. The galvo scanner unit at the sample arm was used to scan the imaging beam over the sample. The reference arm galvo scanner for the phase modulation method has 4.5 mm scanning range on the mirror. In addition, as a separate phase-shifting component we used the piezoelectric translator (P-840.40, Physics Instruments) in the reference arm of the OCT system. The full travel displacement of the PZT was 60 μm when applying 10 V to an open loop PZT amplifier module (x10 amplification). The mirror attached at the PZT has 7 mm diameter and 22.5 grams. A Fourier reconstruction algorithm of the OCT image included DC subtraction and a dispersion compensation method before applying complex conjugate removal procedures. To process the data and display the image, a main computer unit (HP xw8600, 3.2GHz Dual processors) with a rapid speed frame grabber (PCIe 1429, National Instruments) synchronized B-scan timing and sensor exposure timing where the Fd-OCT algorithm programmed with LabVIEW software (National Instruments) was embedded. The galvo scanner and frame grabber were controlled and triggered by a module-based multifunction DAQ (NI PCIe 6363, National Instruments).

2.2 Full-range image reconstruction

The OCT B-scan image including phase shifts can be expressed by

$$I(k,t) = \sum_{z} I_{(x,z)}(k)\cos[\sum_{z}\varphi_{sr}(x,z) + \varphi_{shifting}(t) + \varphi_0] \quad (1)$$

where k is a wave number, $I_{(x,z)}(k)$ is an interference intensity, $\sum_z \varphi_{sr}(x,z)$ is a phase term between the sample and reference arm during scanning, $\varphi_{shifting}(t)$ includes phase shifts both caused by proposed phase modulation and sample motion, and φ_0 denotes an initial phase. Let $\sum_z \varphi_{sr}(x,z) + \varphi_{shifting}(t) + \varphi_0$ substitute to φ_{total}. Fourier transform of the interference fringe $I(k,t)$ into the frequency space produces two symmetric complex conjugate terms as below.

$$FT_{t->\omega}[I(k,t)] = \sum_z I_{(x,z)}(k) \cdot \pi \cdot [\delta(\omega + \varphi_{total}) + \delta(\omega - \varphi_{total})] \tag{2}$$

Equation (2) gives complex conjugate artifact images around a zero frequency line. To eliminate one of the complex conjugate terms, a Heaviside filter scaled by a factor of two, equation (3), was applied to equation (2). Here, scaling by the two preserves the same energy during the filtering process.

$$H(\omega) = \begin{cases} 2, & |\omega - \omega_{shifting}| < \dfrac{B}{2} \\ 0, & otherwise \end{cases} \tag{3}$$

The definition of $\omega_{shifting}$ is an angular frequency (rad/sec) by phase shifts and B is the bandwidth of the Heaviside filter. Fourier filtering of the equation (2) produces a positive side of the complex conjugate value, and then following inverse Fourier transform of the filter output is obtained as the time space below.

$$\bar{I}(k,t) = \sum_z I_{(x,z)}(k) e^{[i(\sum_z \varphi_{sr}(x,z) + \varphi_{shifting}(t) + \varphi_0)]} \tag{4}$$

Finally, inverse Fourier transform of equation (4) into the z space generates the complex conjugate-free image. The Fourier filtering algorithm presented in this paper is similar to the one proposed by Wang [18].

2.3 Suppression ratio and sensitivity

The suppression ratio is the intensity difference between the Fd-OCT sample signal and the complex conjugate suppressed signal. In this study the suppression was obtained after averaging the signal from 20 A-scans to alleviate the effect of random phase fluctuations. The sensitivity of the OCT system was defined by the minimum reflectivity of the sample where the signal was still detected (signal-to-noise ratio equals one) [2]. One can measure the sensitivity drop-off when changing the optical path length between the sample and the reference arm. Figure 2 shows the sensitivity drop-off measured in our Fd-OCT system. The system sensitivity was decreased by 20 dB at a 1.5 mm delay line and the sensitivity has approximately 3 dB difference between 50 fps and 100 fps B-scans. The maximum delay line of our system was ±2mm.

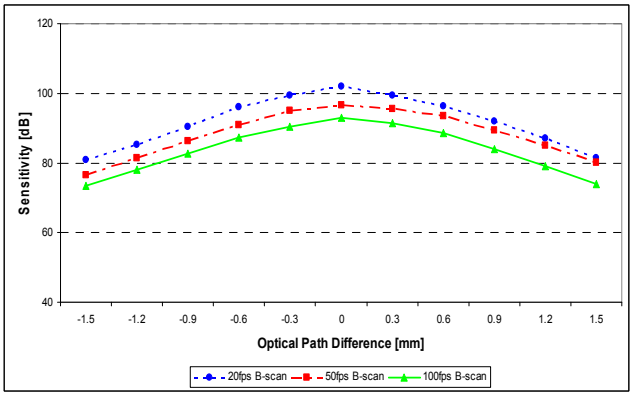

Figure 2. System sensitivity measurement as a function of optical path length difference and at different acquisition speeds.

3 RESULTS AND DISCUSSION

Here we present the suppression ratio of the complex conjugate artifacts resulting from the different phase-shifting methods. Three different exposure times, 8.1, 18 and 47.9 μs were used for image acquisition resulting in 20, 50 and 100 fps for 1000 A-scans. Moreover we show *in vivo* human finger nail images obtained from a standard Fd-OCT reconstruction and a complex ambiguity removal algorithm to compare image quality.

3.1 Suppression ratio

The suppression ratio (SR) is one of the most important criteria for comparing phase-shifting based complex conjugate removal methods. Figure 3 shows the SR of the three different phase-shifting methods using a paperboard at the sample arm. In order to measure the SR of the sample and the reference arm modulation methods, we moved the pivot offset position along a diagonal direction which is a 45 degree angle between the incident beam and the sample or reference mirror. The galvanometer-based phase modulation scans 6 mm at the sample arm and 4.5 mm at the reference arm. For the PZT based method, the SR was obtained by changing applied voltages (0~100 V) which convert the travel length (0~60 μm) of the PZT.

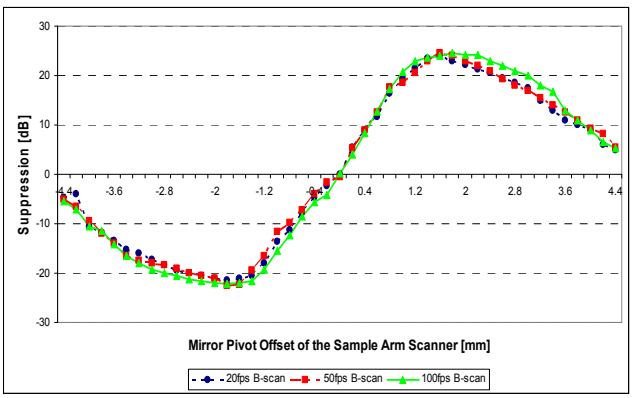

(a)

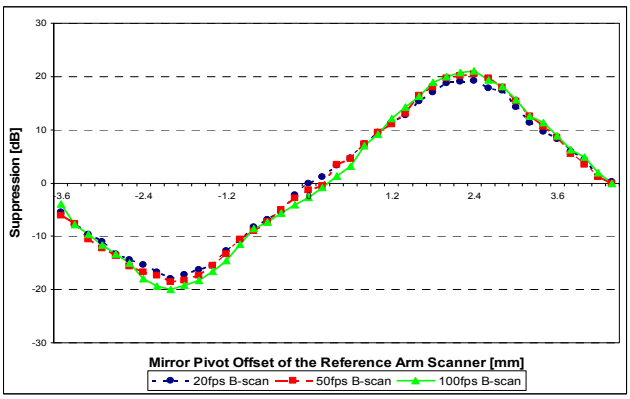

(b)

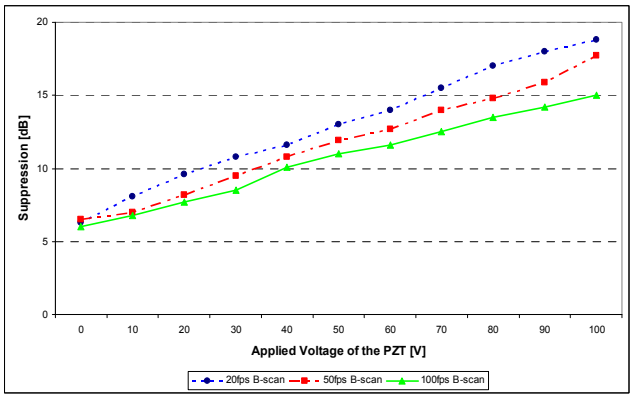

(c)

Figure 3. Suppression ratio of complex conjugate artifacts with: (a) pivot offset scanning of the sample arm, (b) pivot offset scanning of the reference arm, and (c) phase-shifting with the PZT

As shown in Figure 3 (a), the maximum complex conjugate SR was around 25 dB. The phase-shifting between consecutive A-scans was $\Delta\varphi = \frac{\pi}{2}$ and the pivot offset position was 1.6 mm for the sample arm pivot offset scanning. As shown in Figure 3 (a) and (b), the SR of 100 fps B-scan has slightly better suppression than the SR of 20 fps B-scan in both the sample arm and the reference arm pivot-offsetting methods. This may be the reason that high speed galvo

scanning has better phase stability than low speed scanning for the phase-shifting methods. In contrast, the PZT based phase-shifting method has better suppression of the high speed acquisition shown in Figure 3 (c). The phase modulation with the PZT generates approximately 19 dB maximum suppression at 0.45 π of 20 fps B-scan (1000 A-scans) when the PZT travels the full length 60 μm when applying 100 V. However, the PZT method at 50 and 100 fps acquisition results has lower SR than 20 fps B-scan which is mainly caused by the limitation of the actuator stiffness for the loaded condition (mirror attached). However, it is not restricted by the speed of complex conjugate removal operation for the galvo scanner based phase-shifting methods.

3.2 *In vivo* full-range images

To compare image quality for the different phase-shifting schemes, Figure 4 shows standard Fd-OCT images and full-range images for different exposure times. Figure 4 demonstrates B-scan images of human finger pad and nail *in vivo* using the sample arm phase-shifting method according to the different imaging rates. The fast B-scan images, 100 fps, have lower intensity at a finger pad region compared to 20 fps images but it is still possible to discriminate the epidermis and the dermis layers on the finger pad. As shown in Figure 2, the rapid acquisition image has lower sensitivity than the slow acquisition image at the same optical path length. Complex conjugate artifacts are clearly removed for all imaging acquisition speeds using the sample arm phase-shifting method in Figure 4.

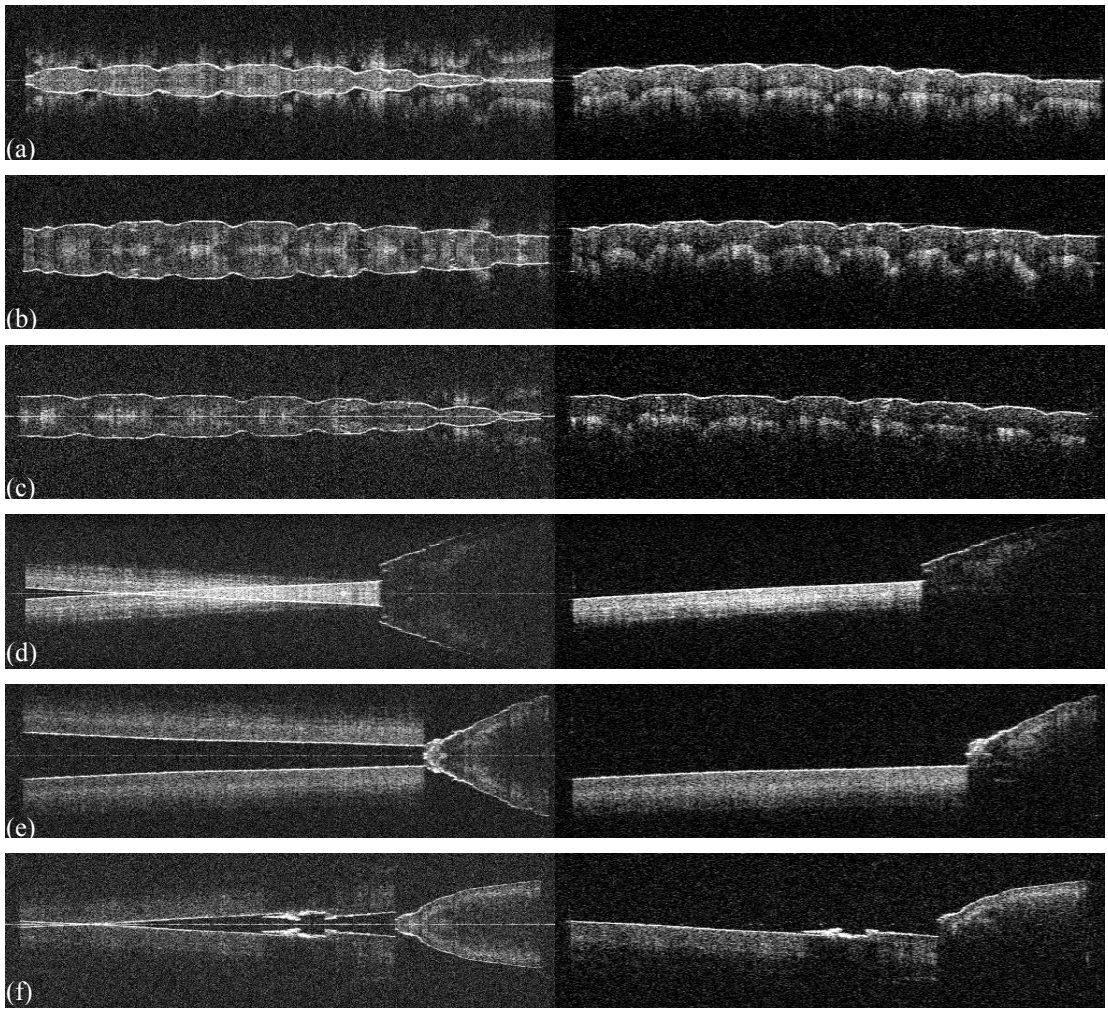

Figure 4. *In vivo* human finger pad and nail images for different image acquisition rates with standard Fd-OCT reconstruction (left) and the phase-shifting ($\Delta\varphi=0.5\pi$) method with the sample arm pivot-offsetting (right). (a)

Finger pad at 20 fps B-scan. (b) Finger pad at 50 fps B-scan. (c) Finger pad at 100 fps B-scan. (d) Finger nail at 20 fps B-scan. (e) Finger nail at 50 fps B-scan. (f) Finger nail at 100 fps B-scan. The image scanning range is 6 mm.

The results shown in Figure 5 are acquired using phase-shifting methods with the reference arm pivot-offsetting method and the PZT phase shift method. Complex conjugate artifact free images acquired at 20 fps in Figure 5 (a) (c) retain some residual structural information which slightly decreases suppression ratio and deteriorates image quality. In addition to the images (a), (c), the reference arm phase modulation methods have higher coherence noise than the sample arm phase modulation method because of reference beam stability. The reference beam intensity variance during scanning requires an additional DC subtraction algorithm to compensate the DC value changes over A-scans. Furthermore the reference arm phase modulation methods demand careful attention to the reference beam alignment for reducing reference beam intensity changes. The fast acquisition images, Figure 5 (b), (d), have better suppression ratio than 20 fps B-scan images. Comparing Figures 4 and 5, one can see that the phase-shifting method of the sample arm has better complex conjugate suppression than that of the sample arm. However, the sample arm phase-shifting complicates implementation in our OCT system with adaptive optics. The maximum phase shifts of the PZT experiment has 0.45π for 1000 A-scans due to the limit of the PZT displacement.

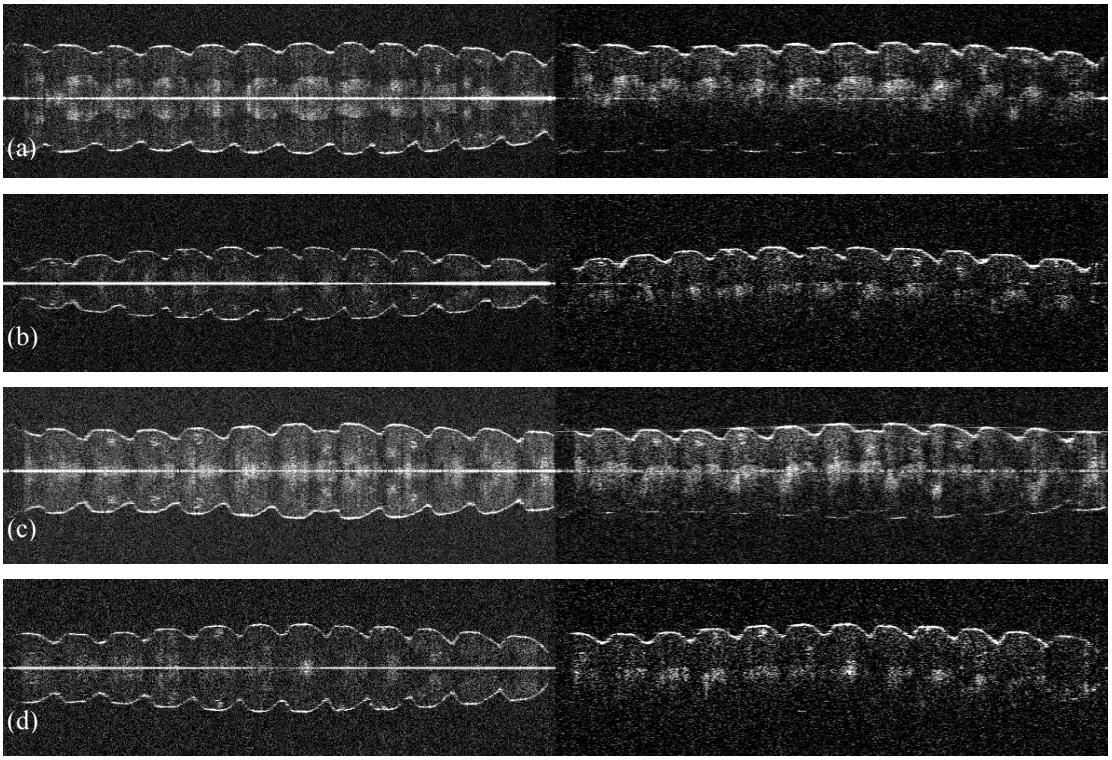

Figure 5. *In vivo* human finger pad images for different phase-shifting methods with standard Fd-OCT reconstruction (left) and full-range image reconstruction (right). (a) 20 fps B-scans with the reference arm pivot offset method ($\Delta\varphi = 0.5\pi$). (b) 100 fps B-scans with the reference arm pivot offset method ($\Delta\varphi = 0.5\pi$). (c) 20 fps B-scans with the PZT based phase-shifting method ($\Delta\varphi = 0.45\pi$). (d) 100 fps B-scans with the PZT based phase-shifting method ($\Delta\varphi = 0.45\pi$). The scanning range of images is 8.5 mm.

4 CONCLUSIONS

We demonstrate three different phase-shifting techniques introduced by pivot offset scanning of the sample arm and the reference arm, as well as phase-shifting with the piezoelectric actuator. The full-range images are acquired by using a Fourier filtering algorithm with the phase-shifting procedure. The maximum suppression ratio is measured when phase-shifting has $\Delta\varphi = 0.5\pi$. Pivot-offsetting of the sample arm scanning technique achieves maximum complex conjugate suppression ratio of nearly 25 dB. There is no restriction in using the high-speed complex conjugate removal method for

the galvo scanner based phase-shifting methods. In the application of adaptive optics Fd-OCT system, the phase-shifting by pivot-offsetting of the reference arm is promising because independent phase modulation is available without any changes in the sample arm.

ACKNOWLEDGEMENTS

This research was supported by the National Eye Institute (EY 014743) and Research to Prevent Blindness.

REFERENCES

[1] M. Wojtkowski, R. Leitgeb, A. Kowalczyk, T. Bajraszewski, and A. F. Fercher " *In vivo* human retinal imaging by Fourier domain optical coherence tomography", J. Biomed. Opt., Vol. **7**, 457 (2002).
[2] R. Leitgeb, C.K. Hitzenberger, and A.F. Fercher "Performance of fourier domain vs. time domain optical coherence tomography", Opt. Express 11, 889-894 (2003).
[3] N. A. Nassif, B. Cense, B.H. Park, M.C. Pierce, S.H. Yun, B.E. Bouma, G.J. Tearney, t.C. Chen, J.F. de Boer "In vivo high-resolution video-rate spectral-domain optical coherence tomography of the human retina and optic nerve", Opt. Express 12, 367-376 (2004).
[4] D. Huang, E. A. Swanson, C. P. Lin, J. S. Schuman, W. G. Stinson, W. Chang, M. R. Hee, T. Flotte, K. Gregory, C. A. Puliafito, and J. G. Fujimoto, Science 254, 1178 (1991).
[5] M. Wojtkowski, A. Kowalczyk, R. Leitgeb, and A. F. Fercher, "Full range complex spectral optical coherence tomography technique in eye imaging," Opt. Lett. 27, 1415-1417 (2002).
[6] R. K. Wang, "In vivo full range complex Fourier domain optical coherence tomography," Applied Physics Letters 90, 054103 (2007).
[7] Y. Yasuno, S. Makita, T. Endo, G. Aoki, M. Itoh, and T. Yatagai, "Simultaneous B-M-mode scanning method for real-time full-range Fourier domain optical coherence tomography," Appl. Opt. 45, 1861-1865 (2006).
[8] Y. K. Tao, M. Zhao, and J. A. Izatt, "High-speed complex conjugate resolved retinal spectral domain optical coherence tomography using sinusoidal phase modulation," Opt. Lett. 32, 2918-2920 (2007).
[9] E. Goetzinger, M. Pircher, R. A. Leitgeb, and C. K. Hitzenberger, "High speed full range complex spectral domain optical coherence tomography," Opt. Express 13, 583-594 (2005).
[10] J. Zhang, J. S. Nelson, and Z. P. Chen, "Removal of a mirror image and enhancement of the signal-to-noise ratio in Fourier-domain optical coherence tomography using an electro-optic phase modulator," Opt. Lett. 30, 147-149 (2005).
[11] A. H. Bachmann, R. A. Leitgeb, and T. Lasser, "Heterodyne Fourier domain optical coherence tomography for full range probing with high axial resolution," Opt. Express 14, 1487-1496 (2006).
[12] B. Baumann, M. Pircher, E. Götzinger, and C.K. Hitzenberger, "Full range complex spectral domain optical coherence tomography without additional phase shifters," Opt. Express 15, 13375-13387 (2007).
[13] L. An and R. K. Wang, "Use of a scanner to modulate spatial interferograms for in vivo full-range Fourier-domain optical coherence tomography," Opt. Lett. **32**, 3423-3425 (2007).
[14] M. Szkulmowski, I. Grulkowski, D. Szlag, A. Szkulmowska, A. Kowalczyk, and M. Wojtkowski, "Flow velocity estimation by complex ambiguity free joint Spectral and Time domain Optical Coherence Tomography," Opt. Express 17, 14281-14297 (2009)
[15] M. V. Sarunic, B. E. Applegate, and J. A. Izatt, "Real-time quadrature projection complex conjugate resolved Fourier domain optical coherence tomography," Opt. Lett. 31, 2426-2428 (2006).
[16] M. V. Sarunic, M. A. Choma, C. H. Yang, and J. A. Izatt, "Instantaneous complex conjugate resolved spectral domain and swept-source OCT using 3x3 fiber couplers," Opt. Express 13, 957-967 (2005).
[17] B. Hofer, B. Považay, B. Hermann, A. Unterhuber, G. Matz, and W. Drexler, "Dispersion encoded full range frequency domain optical coherence tomography," Opt. Express 17, 7-24 (2009).
[18] R. K. Wang, "Fourier domain optical coherence tomography achieves full range complex imaging in vivo by introducing a carrier frequency during scanning", Physics in Medicine and Biology, 52, 5897-5907 (2007)